Heliyon 9 (2023) e13582

Contents lists available at ScienceDirect

Heliyon

journal homepage: www.cell.com/heliyon

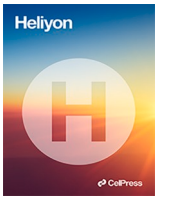

Research article

A semi-empirical formula based on a modified general penetration resistance for predicting the motion of the rigid projectile

Zhao Zhang, Yanqing Wu *, Fenglei Huang **

State Key Laboratory of Explosion Science and Technology, Beijing Institute of Technology, Beijing 100081, PR China

ARTICLE INFO

Keywords:
Penetration
Rigid projectile
Resistance
Semi-empirical formula

ABSTRACT

The semi-empirical formula is an effective method for predicting the motion of rigid projectiles in practical applications due to the simplicity of its theory and the convenience of parameter calibration. The commonly used semi-empirical formula is Forrestal's form, combining several specific experimental cases that have been published, we find it exists deficiencies in predicting deceleration histories and the penetration depths of high velocities. To solve this problem, the general penetration resistance is employed to formulate the semi-empirical formula due to the 'general' characteristic of the general penetration resistance, and also make an assessment of this semi-empirical through experimental data. The results show that this semi-empirical method, like Forrestal's form, is not good at predicting high-velocity penetration depth. Thus, it propels us to develop a new semi-empirical formula. To this end, the general penetration resistance is modified with the assumption that the additional mass should be increased with the penetrating velocity and the projectile mass, based on which a new semi-empirical formula is developed. Then, the proposed semi-empirical formula is employed in individual published experimental data of different projectiles and striking velocities as well as different targets. The predictions of the proposed semi-empirical formula show good agreement with the experimental data both in penetration depths and deceleration histories, which also demonstrate the reasonableness of the assumption that the additional mass of rigid projectile increases with penetrating velocity and the projectile mass.

1. Introduction

Penetration mechanics has received great attention in the industrial and military fields, due to its role in product design and product performance evaluation. Penetration mechanics is a subject full of interest and challenge, studies are usually based on data acquired from experimental observations to understand this problem, further, many theoretical approaches have been developed for making such predictions and they are generally classified into three categories: empirical equations, analytical models and numerical simulations. All those approaches have their strengths and weakness.

Both analytical models and numerical simulations require reasonable constitutive equations of the material that include the shear-failure envelope and the equation of state. Analytical models attempt to adopt a simplified theoretically based constitutive equation aiming at calculating much information on the penetration event based on the simplified assumptions. However, as Yankelevsky [1]

* Corresponding author.
** Corresponding author.
E-mail addresses: wuyqing@bit.edu.cn (Y. Wu), huangfl@bit.edu.cn (F. Huang).

https://doi.org/10.1016/j.heliyon.2023.e13582
Received 3 January 2023; Received in revised form 28 January 2023; Accepted 3 February 2023
Available online 10 February 2023

concluded, those simplified assumptions in the analytical models may not be reasonable in the entire penetration event and may affect the prediction accuracy. Numerical simulations enable to employ of the most complex constitutive formulations and boundary conditions and thus are able to predict more advanced results of the penetration problem. However, it needs a companion experimental of material tests to calibrate the parameter of the constitutive models, which may require special custom devices that exist in a limited number of laboratories. Moreover, the problem that lacking suitable constitutive equations for some targets may be an obstacle to applying the analytical models and the numerical models. Thus, the empirical formula will always be required for proper predictions due to the complexity of the penetration event.

Both the analytical models and numerical simulations can provide information about the response of the target and the projectile, while the empirical formula mainly provides information about the projectile motion. Empirical formulas can be theoretically divided into pure empirical formulas and semi-empirical formulas. The pure empirical formulas are concluded by extensive test data and mainly towards estimating the full penetration depth. Semi-empirical formulas, based on some theories and calibrated by penetration depth data, can predict the motion history information of the projectile as well as the full penetration depth. In actual engineering analysis and design, in addition to the penetration depth, people often want to know the process information, such as deceleration history and velocity history. When there is no acceleration sensor in the test, the process information cannot be obtained from the test. In this paper, the focus is on the motion (penetration depth, deceleration, etc.) of the rigid projectile. Besides, with the development of diverse target materials, the corresponding constitutive equations may become complex, which may cause difficulty in calibrating the material constitutive parameters, in this case, the semi-empirical can serve as an effective method for predicting the motion of rigid projectiles. Thus, attention in this paper is on the semi-empirical formula.

Until now, many semi-empirical formulae have been proposed, which were well summarized in review papers [1,2] and research papers [3–5], and a recent book [6]. The fundamental discrepancy among the different semi-empirical formulae is related to the description of the penetration resistance exerted on the rigid projectile. Besides, with the development of new penetration resistance forms, the correspondingly new semi-empirical formulae can be established.

The simplest resistance form is the constant resistance with only one static resistance parameter a, which was firstly proposed by Robins and Euler [6]. In recent past years, a similar resistance expression was also suggested by Rosenberg et al. through analyzing the numerical simulation results and some penetration experimental data. However, the reasonableness of the constant resistance is under debate, as clearly evident in the papers of [7–11]. The main stand in Refs. [8,10,11] is that the time-deceleration of the projectile is velocity-dependent according to multiple groups of experimental data and numerical data, the contribution of the velocity-dependent term to the total resistance increases with the striking velocity, and the constant resistance is only the natural manifestation in the low-velocity. As seen, the constant resistance encounters some difficulty in predicting the deceleration histories.

Other common penetration resistance forms have a theoretical basis, which can be derived from the cavity expansion theory. The first form is derived by Forrestal et al. [12], who performed the spherical cavity expansion analysis with a simple elastic-plastic constitutive material, the first form is expressed as $\sigma = a+cv^2$, where a is the static resistance, and cv^2 is the dynamic inertial resistance. It should be mentioned that this penetration resistance form was first suggested by French engineer Poncelet [13], and much later by Petry and Goodier [14]. The second form is gained by Warren and Forrestal [15], who introduce a once power of velocity into the Forrestal form by accounting for the strain rate sensitivity and strain hardening in the spherical cavity-expansion approximation. The second resistance form becomes: $\sigma = a+bv + cv^2$. The third form is the general penetration resistance, through which three dimensionless parameters controlling the penetration depth have been concluded by Chen et al. [16], the general penetration resistance is a generalized form of the forms from Warren and Forrestal [15] and from Forrestal et al. [12], i.e., $\sigma = a+bv + cv^2+d\dot{v}$. Compared to the form derived by Warren and Forrestal [15], the general penetration resistance further introduces the term of additional mass. As stated by Chen et al. [16], this general penetration resistance is usually recognized as a general form of penetration resistance, although the penetration resistance can be commonly devised as a series form of instantaneous velocity from the viewpoint of mathematics.

The most commonly used semi-empirical formula in real penetration problems is Forrestal's form, such as applications in concretes with unconfined compressive strengths of 23 MPa [17,20], 39 MPa [17], 58.4 MPa [18], 13.5 MPa and 21.6 MPa [19], and limestone target [21,22]. The penetration events that the large diameter rigid projectiles penetrated into concretes that had an average compressive strength of 39 MPa should be noted, the deceleration results of those tests all show gradual falling trends in the tunnel stage. However, as concluded by Forrestal et al. [17], their formula can not properly predict deceleration histories, the predicted results show large deviations toward the end of the penetration event. Besides, the penetration depth results from Piekutowski et al. [23] for rigid steel rods impacting aluminum 6061 targets and from Feng et al. [24] for rigid steel projectile penetrating concrete with average compressive strength of 47.6 MPa are worth attention. Those two sets of tests feature with a large range of the rigid penetration velocity (up to 1.8 km/s for aluminum and 1.5 km/s for concrete) without any apparent deformation of these projectiles, which is suitable to assess the performance of the semi-empirical formula. As presented in Section 2, Forrestal's form can not properly predict the penetration depths at the large striking velocities. From the above, it can be inferred that Forrestal's form exists the predicted deficiencies both in penetration depths and the deceleration histories.

The above review shows that the constant resistance form and Forrestal's form exhibit the predicted problems in deceleration histories or penetration depths, which propel us to seek a proper semi-empirical formula to solve this problem. Since the general penetration resistance is usually recognized as a general form of penetration resistance, the general penetration resistance is employed to formulate the semi-empirical formula and further examine its predicted ability by combing specific experimental data. It should be noted that, as we know now, no previous investigations have given a careful examination of the general penetration resistance by considering both the entrance stage and the tunnel stage.

This paper is divided into two parts. The first part focuses on evaluating the semi-empirical formula based on general penetration

resistance (denoted as GPR). To this end, the total motion equation of the projectile including both the entrance stage and tunnel stage is established. Then, the performance of GPR is checked by comparing with the specific test data from Piekutowski et al. [23] and Feng et al. [24]. Also, a comparison of Forrestal's form is given. The results, as presented in Section 2, show that both GPR and Forrestal's form can not predict well the experimental penetration depths in the high velocities of the rigid projectile. To solve this problem, the second part is concerned with developing a new semi-empirical formula. The foundation of this new semi-empirical formula is a modified general penetration resistance, which assumes that the additional mass of the projectile should be varied with the penetrating velocity and the projectile mass rather than a constant in the original general penetration resistance. The detailed description of our assumption and the new semi-empirical formula based on the modified general penetration resistance (denoted as NGPR) are presented in Section 3. In Section 4, the predictions by NGPR are compared with individual published experimental data of different projectiles and striking velocities as well as different targets. For the comparison, the proposed semi-empirical model is compared with the GPR formula. The better agreement of predictions by NGPR with test results demonstrates the good performance of this new semi-empirical formula and the reasonableness of the assumption that the additional mass of projectile varies with penetrating velocity and the projectile mass.

2. Evaluation of the semi-empirical formula based on the general penetration resistance

2.1. Equation of the rigid projectile motion

The penetration process can be divided into two stages: the entrance stage and the tunnel stage. Many formulae [2,20,18] assume that the depth of the entrance stage should be equal to the two-six diameters of the projectile. However, as discussed by Yankelevsky and Feldgun [25], the above assumptions about the depth of the entrance stage are ambiguous and can not account for the nose slenderness. Thus, they postulated that the depth of the entrance stage should be equal to the length of the projectile nose rather than the commonly used two-six diameters of the projectile. Then, they integrated the radial cavity pressure on a "projectile-target" variable contact area which is increasing with time during the entrance stage to represent the resistance during the entrance stage. Their postulate was validated by the deceleration recorded data from penetration tests using instrumented projectiles. Here, we adopt their new description of the depth of the entrance stage, in order to simplify the analysis, the linear deceleration relationship that the Forrestal's formulae assumed [17] is still used to describe the entrance stage. The motion equation of the rigid projectile in the tunnel stage is formulated by using the general penetration resistance.

A rigid projectile with a common convex nose shape, as shown in Fig. 1, normally impacts a target at initial velocity v_s and proceeds to penetrate the target at velocity v. The axial resistance force acting on the projectile during the entrance stage is expressed as:

$$M\frac{dv}{dt} = M\frac{d^2x}{dt^2} = F_x = -kx, \quad 0 < x < L \tag{1}$$

where k is a constant.

The condition of $x = L$ means the end of the entrance stage and the beginning of the tunnel stage. The motion equation of the rigid projectile in the tunnel stage is formulated by the general penetration resistance which expresses a relationship between the normal compressive stress σ_n on the projectile nose and the normal expansion velocity v_n [16]:

$$\sigma_n = AY + C\sqrt{\rho Y}v_n + B\rho {v_n}^2 + D\rho d\dot{v}_n \tag{2}$$

where d is the diameter of the projectile, Y and ρ are yielding stress and density of target material, respectively. Specifically, for concretes and metals concerned in this paper, Y represents the yield stress and the unconfined compressive strength f_c, respectively. The dimensionless parameters A, B, C and D control the effect of target resistance, target inertia, target damping and the additional mass, respectively. The general penetration resistance of Eq. (2) reduces to Forrestal's form with parameters C and D equal to zero. In the case of $D = 0$, the formula derived by Warren and Forrestal [15] can be obtained.

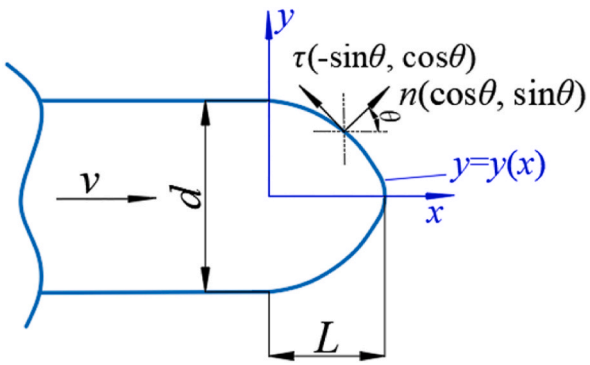

Fig. 1. Penetration of a general nose-shape projectile.

The cavity normal expansion particle velocity induced by the rigid projectile with velocity v is:

$$v_n = v\cos\theta \tag{3a}$$

$$\dot{v}_n = \dot{v}\cos\theta \tag{3b}$$

According to Fig. 1, the total axial resistance force on the projectile can be gained by integration of the normal compressive stress and the tangential stress along the projectile nose surface :

$$F_x = \iint(\sigma_n\cos\theta - \sigma_t\sin\theta)\mathrm{d}A_s = \oint\sigma_n(\cos\theta + \mu_m\sin\theta)\mathrm{d}A_s \tag{4}$$

where A_s is the nose area of the rigid projectile. Tangential stress on the nose is determined by the frictional resistance, i.e., $\sigma_t = -\mu_m\sigma_n$, where μ_m is the sliding friction coefficient in impact.

Insertion of Eq. (2) and Eq. (3) into Eq. (4), and integration of Eq. (4) can provide:

$$F_x = \frac{\pi d^2}{4}\left[AYN_1 + B\rho v^2N_2 + \left(C\sqrt{\rho Y}\,v + D\rho d\dot{v}\right)N_3\right] \tag{5}$$

where N_1, N_2, and N_3 are three dimensionless parameters used to characterize the nose shape and friction. N_1, N_2, and N_3 have been defined in Chen et al. [16]. For the nose profile that can be expressed by the general convex function $y = y(x)$, N_1, N_2, and N_3 need to be obtained through numerical integration, while for the commonly used ogival nose, conical nose and spherical nose in weapon engineering, N_1, N_2, and N_3 have explicit expressions. Appendix A provides the expressions of N_1, N_2, and N_3 for the general convex noses and commonly used typical noses.

equation (5) can be rewritten as:

$$M_m\frac{dv}{dt} = M_mv\frac{dv}{dx} = -\frac{\pi d^2}{4}\left(AYN_1 + B\rho v^2N_2 + C\sqrt{\rho Y}\,vN_3\right) \tag{6}$$

The projectile mass M is modified as M_m after taking the effect of additional mass into consideration:

$$M_m = M + \frac{\pi\rho d^3}{4}DN_3 = M + M_a \tag{7}$$

Eq. (6) can be further rewritten as:

$$M\frac{dv}{dt} = -\frac{M}{M_m}\frac{\pi d^2}{4}\left(AYN_1 + B\rho v^2N_2 + C\sqrt{\rho Y}\,vN_3\right) \tag{8}$$

It can be seen from Eq. (8) that when the additional mass is considered, the target resistance is weakened, which results in a deeper penetration depth.

The penetration depth can be determined through integration of Eq. (6) as below:

$$\frac{\pi d^2}{4M_m}\int_L^P dz = \int_0^{v_1}\frac{vdv}{\left(AYN_1 + B\rho v^2N_2 + C\sqrt{\rho Y}\,vN_3\right)} \tag{9}$$

In Eq. (9), v_1 is the initial velocity of the tunnel stage and v_1 can be determined through deceleration continuous condition at $x = L$, the detail derivation of v_1 will be given later. Referring to the integration approach of Chen et al. [16], the penetration depth P can be obtained analytically as below:

$$P = \frac{2}{\pi}N\left\{\ln\left(1 + 2\sqrt{\xi\frac{I}{N}} + \frac{I}{N}\right) - \frac{2\sqrt{\xi}}{\sqrt{1-\xi}}\left[\arctan\left(\frac{\sqrt{I/N} + \sqrt{\xi}}{\sqrt{1-\xi}}\right) - \arctan\left(\frac{\sqrt{\xi}}{\sqrt{1-\xi}}\right)\right]\right\}d + L \quad 0 \le \xi < 1 \tag{10a}$$

where

$$I = \frac{M_mv_1^2}{d^3YAN_1} \tag{10b}$$

$$N = \frac{M_m}{\rho d^3BN_2} \tag{10c}$$

$$\xi = \frac{C^2N_3^2}{4ABN_1N_2} \tag{10d}$$

$$M_m = M + \frac{\pi\rho d^3}{4}DN_3 \tag{10e}$$

where I is the dimensionless impact function, N is the geometry function, ξ is dimensionless damping function. According to the

discussion of Chen et al. [16], the penetration depth has real physical meaning only when ξ is less than one, thus the integration result of Eq. (9) with ξ greater than one is not given here.

Now, it turns to the derivation of the initial velocity v_1 of the tunnel stage, which is also the velocity at the end of the entrance stage. With the initial conditions $x(t=0)=0$ and $v(t=0)=v_s$, Eq. (1) has the following solutions for projectile displacement, velocity, and deceleration:

$$z=\left(\frac{v_s}{w}\right)\sin wt, 0<x<L \tag{11a}$$

$$v=v_s\cos wt, 0<x<L \tag{11b}$$

$$\frac{\mathrm{d}v}{\mathrm{d}t}=-wv_s\sin wt, 0<x<L \tag{11c}$$

$$w^2=\frac{k}{M_m} \tag{11d}$$

Note that in Eq. (11d), the additional mass M_m is used rather than M, which can ensure the additional mass of the projectile in the tunnel phase is the same as that in the entrance phase. Define t_1 as the time at $x=L$, from Eq. (11a) and Eq. (11b):

$$L=\left(\frac{v_s}{w}\right)\sin wt_1, at \quad x=L \tag{12a}$$

$$v_1=v_s\cos wt_1, at \quad x=L \tag{12b}$$

Squaring Eq. (12a) and Eq. (12b), and then adding gives:

$$M_m\left(v_s^2-v_1^2\right)=kL^2 \tag{13}$$

Substituting Eq. (13) into Eq. (1) yields:

$$F(x=L)=-\frac{M_m\left(v_s^2-v_1^2\right)}{L} \tag{14}$$

Equating Eq. (14) with Eq. (6) at $x=L$ yields:

$$\frac{M_m\left(v_s^2-v_1^2\right)}{L}=\frac{\pi d^2}{4}\left(AYN_1+B\rho {v_1}^2N_2+C\sqrt{\rho Y}\,v_1N_3\right), at \quad x=L \tag{15}$$

Value of v_1 can be determined from Eq. (15):

$$v_1=\frac{-CN_3\sqrt{\rho Y}+\sqrt{\left(C\sqrt{\rho Y}\right)^2{N_3}^2-4\left(\rho BN_2+\frac{4M_m}{\pi d^2L}\right)\left(AYN_1-\frac{4M_m}{\pi d^2L}v_s^2\right)}}{2\left(\rho BN_2+\frac{4M_m}{\pi d^2L}\right)} \tag{16}$$

Then, k can be obtained from Eq. (13), further, ω can be obtained from Eq. (11d).

Placing Eq. (16) into Eq. 10(a-e), an explicit relationship between the penetration depth (P) and the initial striking velocity (v_s) can be obtained as follow:

$$P=\frac{2}{\pi}N\left\{\ln\left(1+2\sqrt{\xi\frac{I}{N}}+\frac{I}{N}\right)-\frac{2\sqrt{\xi}}{\sqrt{1-\xi}}\left[\arctan\left(\frac{\sqrt{I/N}+\sqrt{\xi}}{\sqrt{1-\xi}}\right)-\arctan\left(\frac{\sqrt{\xi}}{\sqrt{1-\xi}}\right)\right]\right\}d+L \quad 0\le\xi<1 \tag{17a}$$

where

$$I=\frac{M_m{v_1}^2}{d^3YAN_1} \tag{17b}$$

$$N=\frac{M_m}{\rho d^3BN_2} \tag{17c}$$

$$\xi=\frac{C^2N_3^2}{4ABN_1N_2} \tag{17d}$$

$$M_m=M+\frac{\pi\rho d^3}{4}DN_3=M+M_a \tag{17e}$$

$$v_1 = \frac{-CN_3\sqrt{\rho Y} + \sqrt{\left(C\sqrt{\rho Y}\right)^2 N_3{}^2 - 4\left(\rho BN_2 + \frac{4M_m}{\pi d^2 L}\right)\left(AYN_1 - \frac{4M_m}{\pi d^2 L}v_s^2\right)}}{2\left(\rho BN_2 + \frac{4M_m}{\pi d^2 L}\right)} \tag{17f}$$

As can be seen, there are four parameters A, B, C, and D in the formula of Eq.17(a-f). Once four parameters are determined, the penetration depth at arbitrary velocity can be obtained in the condition of rigid penetration. The deceleration history of the projectile in the entrance stage can be directly obtained from Eq. (11c), and that in the tunnel stage can be numerically solved from Eq. (5). Further, the velocity history and displacement history can be obtained by once and double integration of the deceleration-time relation, respectively.

There are two methods to determine the values of the four parameters. The first method is using the dynamic cavity-expansion theory to analytically or numerically determine the parameters A, B, and C, but the parameter D can not yet be determined using this way, besides, how theoretically determining the value of D is still an unsolved issue. In the second method, Eq.17(a-f) is treated as a semi-empirical formula, the four parameters can be determined by optimizing the penetration results of penetration depth verse impact velocity. The focus of this paper is on the semi-empirical formula, thus the second method will be used to determine the parameters. The following optimization function is employed to minimize the average error:

$$\underset{(A,B,C,D)}{Min}\,(Error)_{av} = \underset{(A,B,C,D)}{Min}\sum_{i=1}^{N} P_i^{Pred}\left(\frac{P_i^{Pred}}{P_i^{ex}} - 1\right)^2 \tag{18}$$

where N is the total number of data points. When using the optimization method, the value range of parameters A, B, C, and D should be given. Here, to produce reasonable values of parameters, the range of each parameter is presented by referring to the published value of A, B, and C from cavity expansion theory. For concrete and aluminum alloy concerned in this paper, previous studies [12,23,26,27] show that B relates mostly to the compressibility of the target material and has a narrow range, generally, the range of B is from 1.0 to 1.3. In contrast, parameter A has a broad range. The parameter A_u gained by calibrating the experimental penetration depth data based on assumption of the constant resistance is regarded as the upper limit of the parameter A, this is because the velocity dependent terms in general penetration resistance of Eq. (2) also provide the contribution on the total resistance. As for parameter C, its limit can be indirectly controlled through the damping parameter ξ of Eq. (17d). Chen et al. [16] concluded that ξ is a small value and sometimes approaches zero for the penetration experiments that this paper referenced here. According to the published values of A, B, and C from the cavity expansion model, ξ is less than 0.1 for aluminum alloys [15], and ξ is less than 0.2 for concrete [28]. Due to no published theoretical value can be referenced for parameter D, its range is not limited here.

For ease of reference, the formula based on general penetration resistance is denoted as the GPR formula. The next section gives applications of this GPR formula on the penetration data from Piekutowski et al. [23] and Feng et al. [24], a comparison of Forrestal's form is also given.

2.2. Evaluation of the GPR formula and Forrestal's form

A lot of experimental data on deep penetration of rigid projectiles with different nose shapes have been reported over the past several decades. The penetration data from Piekutowski et al. [23] and Feng et al. [24] are preferentially considered to check the predicted ability of the GPR formula and the Forrestal's form, this is because the rigid penetration velocity in these two sets of penetration tests is in a large range. One point should be mentioned is the effect of friction on the penetration depth. As concluded by

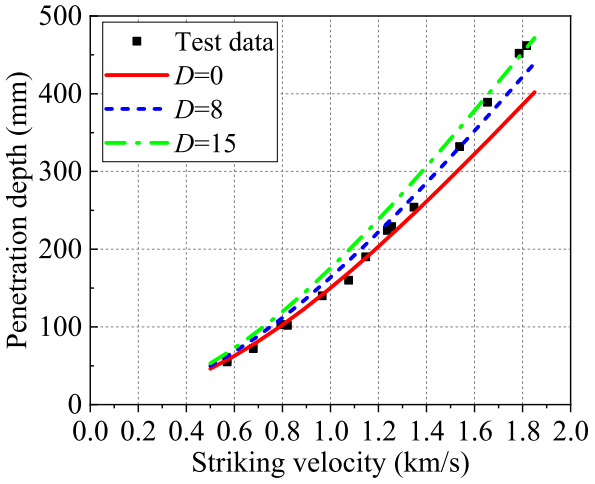

Fig. 2. The predicted penetration depths of Al 6061 penetration [23] using the GPR formula with different additional mass.

Rosenberg [29,30], the effect of friction on the shanks of rigid sharp-nosed projectiles can be neglected for the deep penetration of the metal and concrete targets. Thus, it can be inferred that the friction of the projectile nose mainly affects the penetration depth. However, how to ahead quantify a proper friction coefficient or friction coefficient function is still an unsolved problem. In the remainder of this paper, for aluminum alloys, we follow the suggested friction coefficient in Forrestal et al. [12], that is $\mu_m = 0.02$ for ogive nose and $\mu_m = 0.1$ for conical nose and sphere nose; for concretes, keep the same setting as for aluminum alloys.

In the penetration event by Piekutowski et al. [23], the projectiles had a shank diameter of 7.11 mm, a nominal mass of 0.021 kg and an ogive nose shape with 3.0 Caliber-Radius-Head (CRH). The projectiles shot normally at 6061-T651 aluminum targets with a static yield strength of 276 MPa at an impact velocity of 0.5 km/s-1.8 km/s without apparent deformation. Piekutowski et al. [23] provided values of A, B, and C from cavity expansion model which considers the compressible property, strain hardening and strain-rate sensitivity, i.e., $A = 5.04$, $B = 0.983$, and $C = 0.94$. Based on this group of parameters, the predicted penetration depths from the GPR formula with different values of D is depicted in Fig. 2. As can be seen, when the additional mass is small, the predictions of GPR fit well with the penetration depth of the low-middle velocity section, but poorly with the penetration depth of the high-velocity section. An opposite trend is presented when the additional mass becomes large. The predictions with D equals to 15.0 and 0.0 are the upper and lower envelopes of test data, respectively. Regardless of any value of D, the predictions from the GPR formula can not fit well all the experimental data points.

By using values of parameters from the cavity expansion model, it is concluded that the GPR formula can not correctly predict the penetration depth. Now, the GPR formula is further checked by using the optimization method, that is, the GPR formula is treated as a semi-empirical formula. In fact, the optimization method can essentially reflect the predicted ability of a formula due to its parameters are determined by optimizing with the data points.

By reducing the error function of Eq. (18) with the test data in Piekutowski et al. [23], the four parameters in the GPR formula are optimized to be $A = 6.22$, $B = 1.0$, $C = 0$, $D = 13.2$. The corresponding predicted penetration depths with the semi-empirical GPR formula are depicted in Fig. 3. Also, the predicted results from Forrestal's form are presented. It is obvious that both the GPR formula and Forrestal's formula are not able to correctly reflect the penetration depths at high velocities.

Then, the penetration event performed by Feng et al. [24] is utilized to further evaluate the predicted ability of the GPR formula and Forrestal' form. Feng et al. [24] conducted seven penetration tests with concrete that had an average compressive strength of 47.6 MPa at initial striking velocities from 841 m/s to 1402 m/s. All the projectiles were characterized with 3.0 Caliber-Radius-Head (CRH) and 60 mm diameter. Also, projectiles of those tests were regarded as rigid bodies since the mass loss and deformation of projectiles were relatively less. Since no values of parameters from the cavity expansion model were given, parameters of the GPR formula are determined by using the optimization method. With the test data in Feng et al. [24] and error function Eq. (18), the four parameters are optimized to be $A = 10.27$; $B = 1.0$; $C = 0$; $D = 11.09$; The predicted penetration depths with the semi-empirical GPR formula as well as the predictions from Forrestal's form are depicted in Fig. 4. It is observed that the above two semi-empirical formulas can not properly reflect the penetration depth at the high velocity of the rigid projectile.

From the above two classical penetration events, it is concluded that both the GPR formula and Forrestal's formula predict a large error on the penetration depths at larger velocities. To deal with this problem, the general penetration resistance is modified, based on which a new semi-empirical formula is developed, as discussed in the next section.

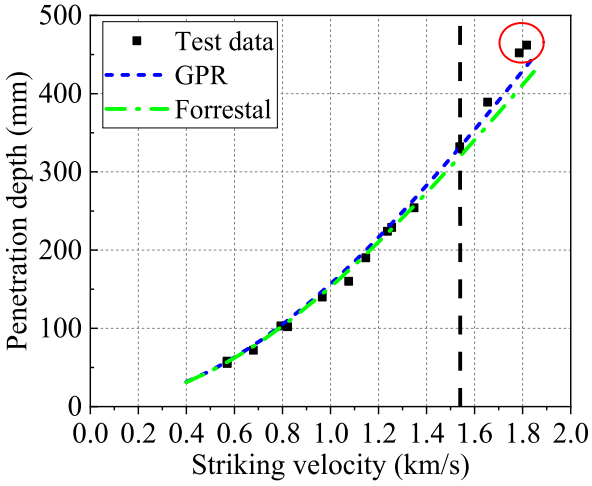

Fig. 3. Comparison between the test data of Al6061 penetration [23] and the predicted penetration depths from the GPR formula and Forrestal's formula.

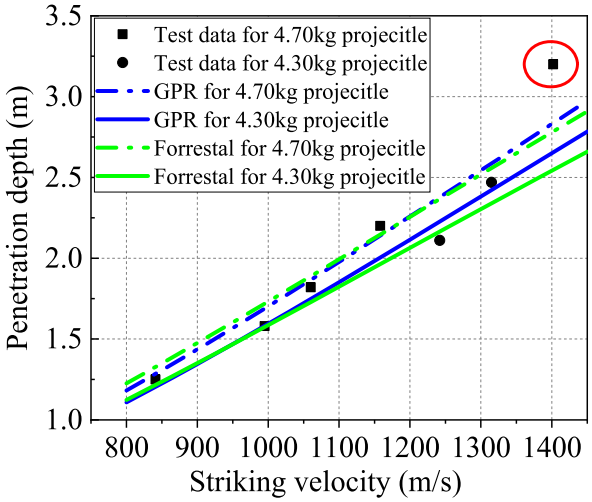

Fig. 4. Comparison between the test data of 47.6 MPa concrete penetration [24] and the predicted penetration depths from the GPR formula and Forrestal's formula.

3. Proposal of a new semi-empirical formula

3.1. The conjecture about the additional mass

Fig. 2 indicates that the additional mass in the GPR formula can not balance the penetration depths in the whole striking velocities. The good fit of the predicted penetration depth to the high-velocity test data will cause a deviation of the predicted penetration depth from the low-velocity test data. With the parameters of GPR formula determined by the optimization method, Figs. 3 and 4 illustrate that the GPR formula is inherently inaccurate in predicting penetration depths at high velocities.

Based on the general penetration resistance, Chen et al. [16] concluded that the penetration depth is controlled by three dimensionless functions, ie., the impact function I, the geometric function N and the damping function ξ, besides, the additional mass as expressed by Eq. (7) is concluded. Also, Chen et al. [16] discussed that, with the increase of the striking velocity, the material flow of the target becomes more obvious and more additional mass should be considered, which is beneficial for predicting a larger penetration depth under the higher striking velocity. Obviously, the viewpoint of Chen et al. [16] is helpful to solve the deviation between predictions by the GPR formula and the test data. However, the additional mass term as expressed by Eq. (7) for a given projectile and target is a constant with no relation to the velocity of the projectile, which indicates that the magnitude of striking velocity has no effect on the flow extent of the target material. Obviously, the additional mass description in the GPR formula contradicts the discussion by Chen et al. [16], which results in the deviation between the predictions by the GPR formula and the test data at the higher striking velocity as shown in Figs. 3–4. From above, it appears that the assumption that the additional mass increases with the striking velocity is supported.

Further, from Eq. (7), the additional mass M_a accounts for the effect of the diameter of the projectile and the geometric of projectile nose but neglects the effect of the projectile mass. Imaging the condition where projectiles have the same diameter, nose shape, and initial striking velocity but different projectile lengths resulting in different masses, obviously the projectile with a larger mass is accompanied by a larger kinetic energy. Following the above discussion by Chen et al. [16], the projectile with a larger kinetic energy can result in a more obvious flow of the target and thus more additional mass. In short, in the condition of projectiles with the same diameter, nose shape, and initial striking velocity, the projectile with a larger mass induces a larger additional mass. However, this point can not be reflected by the additional mass M_a in Eq. (7). In other words, the additional mass M_a in Eq. (7) also needs consider the effect of the projectile mass.

In conclusion, based on the viewpoint of Chen et al. [16], the additional mass M_a expressed in Eq. (7) in the GPR formula needs further consideration of the effects of the striking velocity and the projectile mass. Along with this thought, the modified general penetration resistance is proposed in the next subsection.

3.2. Modification of the general penetration resistance

Generally, the additional mass varies continuously with the velocity of the projectile during penetration, thus it is natural to think the parameter D in Eq. (7) should change with the penetrating velocity v. However, since there is not a rigorous function of D, we may claim that any function forms of the parameter D which express a directly proportional relationship with the penetrating velocity v are reasonable, an example is shown by Eq. (19a). Further, for mathematically easy to process, it is assumed that the parameter D is varied with the initial striking velocity v_s, this assumption means an average additional mass during the whole penetration process for a given initial striking velocity v_s. Besides, considering that the parameter D is dimensionless, it is postulated that the parameter D is a function

of the dimensionless Johnson damage parameter Φ_J as Eq. (19b).

$$D = D(v) = \overline{D}\left(\frac{\rho v^2}{Y}\right)^n \tag{19a}$$

$$D = D(v_s) = \overline{D}\Phi_J = \overline{D}\left(\frac{\rho {v_s}^2}{Y}\right)^n \tag{19b}$$

Eq. (19b) has two parameters $\overline{D}$ and n, with which various increasing trends of the additional mass with striking velocities can be obtained. Insertion of Eq. (19b) into Eq. (2), a modified general penetration resistance is obtained:

$$\begin{aligned}\sigma_n &= AY + C\sqrt{\rho Y}v_n + B\rho {v_n}^2 + D\rho d\dot{v}_n \\ &= AY + C\sqrt{\rho Y}v_n + B\rho v_n^2 + \overline{D}\left(\frac{\rho v_s^2}{Y}\right)^n \rho d\dot{v}_n\end{aligned} \tag{20}$$

It is observed that, the modified general penetration resistance of Eq. (20) reduces to original general penetration resistance of Eq. (2) in the condition of $n = 0$.

Besides, considering the additional mass M_a in Eq. (7) increases with the projectile mass, the original general penetration resistance of Eq. (2) is modified as:

$$\sigma_n = AY + C\sqrt{\rho Y}v_n + B\rho {v_n}^2 + D\rho L_{eff}\dot{v}_n \quad \text{where} \quad L_{eff} = \frac{4M}{\pi d^2} \tag{21}$$

With Eq. (21), following the same derivation in Section 2, the additional mass term becomes:

$$M_m = M + \frac{\pi\rho d^2 L_{eff}}{4} DN_3 = M + MDN_3 = M + M_a \tag{22}$$

As seen in Eq. (22), the additional mass M_a increases with the projectile mass can be correctly reflected.

Finally, in order to comprehensively account for the effect of the striking velocity and the projectile mass on the additional mass, Eq. (20) and Eq. (21) is combined and the modified general penetration resistance is expressed as:

$$\sigma_n = AY + C\sqrt{\rho Y}v_n + B\rho {v_n}^2 + \overline{D}\left(\frac{\rho v_s^2}{Y}\right)^n \rho L_{eff}\dot{v}_n, \text{where} \quad L_{eff} = \frac{4M}{\pi d^2} \tag{23}$$

3.3. Formulation of a new semi-empirical based on a modified general target resistance

Based on the modified general penetration resistance of Eq. (23) and the same derivation process in Section 2, an explicit relationship between the penetration depth (P) and the initial striking velocity(v_s) can be obtained as follow:

$$P = \frac{2}{\pi}N\left\{\ln\left(1 + 2\sqrt{\xi\frac{I}{N}} + \frac{I}{N}\right) - \frac{2\sqrt{\xi}}{\sqrt{1-\xi}}\left[\arctan\left(\frac{\sqrt{I/N} + \sqrt{\xi}}{\sqrt{1-\xi}}\right) - \arctan\left(\frac{\sqrt{\xi}}{\sqrt{1-\xi}}\right)\right]\right\}d + L \quad 0 \le \xi < 1 \tag{24a}$$

where

$$I = \frac{M_m v_1^2}{d^3 YAN_1} \tag{24b}$$

$$N = \frac{M_m}{\rho d^3 BN_2} \tag{24c}$$

$$\xi = \frac{C^2 N_3^2}{4ABN_1 N_2} \tag{24d}$$

$$M_m = M + \frac{M}{4}\overline{D}\left(\frac{\rho v_s^2}{Y}\right)^n N_3 = M + M_a \tag{24e}$$

$$v_1 = \frac{-CN_2\sqrt{\rho Y} + \sqrt{\left(C\sqrt{\rho Y}\right)^2 N_2^2 - 4\left(BN_1\rho + \frac{4M_m}{\pi d^2 L}\right)\left(AY - \frac{4M_m}{\pi d^2 L}v_s^2\right)}}{2\left(BN_1\rho + \frac{4M_m}{\pi d^2 L}\right)} \tag{24f}$$

Through comparison between Eq.17(a-f) and Eq. 24(a-f), it can be seen that only the additional mass term is updated from Eq. (17e) to Eq. (24e). It should be noted that the additional mass M_a in Eq. (24e) is able to reflect the effect of striking velocity and projectile mass. The new expressions for k and ω are the same with Eq. (13) and Eq. (11d) respectively, only the term M_m is updated by Eq. (24e). The deceleration history of the projectile in the entrance and tunnel stage can also be obtained from Eq. (11c) and Eq. (5), respectively.

For ease of reference, this new formula based on the modified general penetration resistance of Eq. 24(a-f) is denoted as the NGPR formula. The NGPR formula can be regarded as a semi-empirical formula if its parameters are determined by optimizing the penetration depth data.

To simplify the unknown parameters, the value of n is set to 1.0. According to Eq. (24e), it means that the additional mass is linearly related to the projectile kinetic energy. The other four parameters A, B, C and $\overline{D}$ are determined by optimizing the data points of penetration depth data verse striking velocity. As will be presented in Section 4, the value of n equals 1.0 is reasonable, because the predictions of the semi-empirical NGPR formula exhibit good agreement with all the referenced experimental data both in penetration depths and deceleration histories.

4. Comparisons between predictions of the NGPR formula with experimental penetration data

In this section, a collection of experimental data from individual published references is employed to evaluate the performance of the NGPR formula. Only the experimental results belonging to the penetration of rigid projectiles are referenced. For the comparison, the NGPR formula is compared with the GPR formula. Here, the NGPR formula and GPR formula are viewed as semi-empirical formulas, thus the parameters of those formulas are determined by optimizing the experimental data points of penetration depth verse striking velocity with Eq. (18). The advantage of the optimization method is that it can essentially reflect the predictive performance of different formulas. The value range for each parameter in the NGPR and GPR formulas is consistent with the description in Section 2.1. It should be mentioned that the GPR formula is the general form of the Forrestal's form, the GPR formula can embody and sometimes is superior to the predictive performance of the latter formula, thus, the Forrestal's form is not included here to avoid redundant comparison. The setting of the friction coefficient is the same as that described in Section 2.2.

4.1. Deep penetration in aluminum alloys

Here, the experimental data of Piekutowski et al. [23], Forrestal et al. [12,27] are utilized. The brief description of the penetration event of Piekutowski et al. [23] can be seen in Section 2.2. For the penetration event of Al7075 in Forrestal et al. [27], the target had a strength of 448 MPa, the projectiles were characterized with 7.11 mm diameter, 0.0248 kg mass, and an ogive nose shape with 3.0 CRH. For the penetration event of the Al6061 target in Forrestal et al. [11], the target had a strength of 400 MPa, the projectiles were characterized with 7.10 mm diameter, 0.024 kg mass, and three nose shapes (ogive shape with 3.0 CRH, semi-sphere nose, and conical nose). Table 1 lists the optimized parameters of the NGPR and GPR formulae corresponding to those aluminum alloy penetration events.

Figs. 5 and 6 show the predictions of the NGPR and GPR formulae and the experimental penetration depths. From Fig. 5, the NGPR formula exhibits a better agreement with the penetration depth data of Al6061 [23] than the GPR formula. From Fig. 6, the NGPR formula presents a similar predicted performance to the GPR formula for the given experimental penetration depths data points of Al7075 [27], but their difference gradually becomes obvious when the striking velocity is further larger. Fig. 7 shows the predictions of the NGPR formula and experimental penetration depths of Al6061 [12] for different projectile noses. The experimental penetration depths of the ogive nose are used to determine the parameters of the NGPR formula, and those parameters are used to predict the penetration depth of the other two nose shapes. Obviously, good agreement is obtained between the predictions and penetration depth test data for all three nose shapes, which reflects that the obtained parameters by optimizing the penetration depths data points are reasonable.

4.2. Deep penetration in concrete

This section performed an analysis on the experimental data of penetration into concrete target. The test data of Feng et al. [24] and Forrestal et al. [17,19] and predictions of the NGPR and GPR formulae are regrouped. The brief description of penetration event in Feng et al. [24] can be seen in Section 2.2. For the penetration events in Forrestal et al. [17], two sets of penetration experiments with concrete targets that had average compressive strengths of 23 MPa and 39 MPa were conducted, the 4340 projectiles were characterized with 7.62 cm diameter, 13 kg mass, and two types of ogive nose shape with 3.0 CRH and 6.0 CRH. For the penetration event in Ref. [19], the concrete target had an average compressive strength of 51 MPa, the 4340 steel projectiles were characterized with 30.5 mm diameter, 1.6 kg mass, and an ogive nose shape with 3.0 CRH. Table 2 lists the optimized parameters of NGPR and GPR formulae corresponding to those concrete penetration events.

Table 1
Optimized parameters of GPR and NGPR formulae for penetration of Al6061 and Al7075.

Target species	Formula	A	B	C	D ($\overline{D}$)
Al6061 [23]	NGPR	5.22	1.29	1.78	0.04
	GPR	6.22	1.0	0.0	13.2
Al7075 [27]	NGPR	4.60	1.22	1.63	0.07
	GPR	5.01	1.0	0.0	7.05
Al6061 [12]	NGPR	3.86	1.23	1.50	0.05
	GPR	4.56	1.0	0.0	10.76

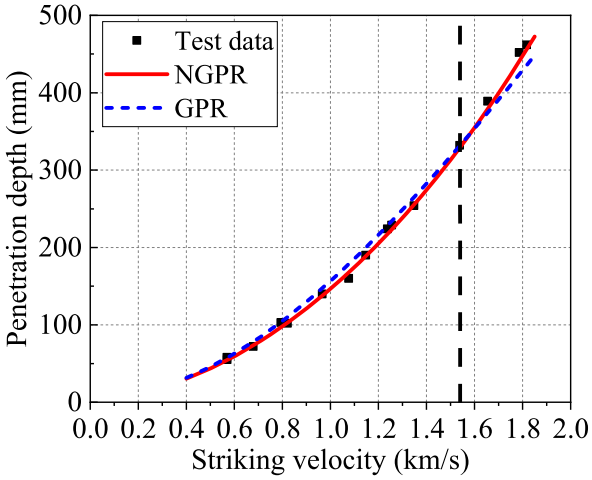

Fig. 5. The depth measurements of penetration Al6061 [23] with the predictions from the NGPR and GPR formulae.

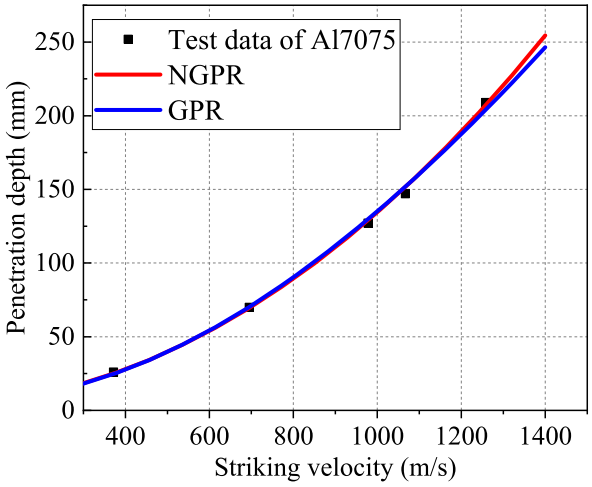

Fig. 6. The depth measurements of penetration Al7075 [27] with the predictions from the NGPR and GPR formulae.

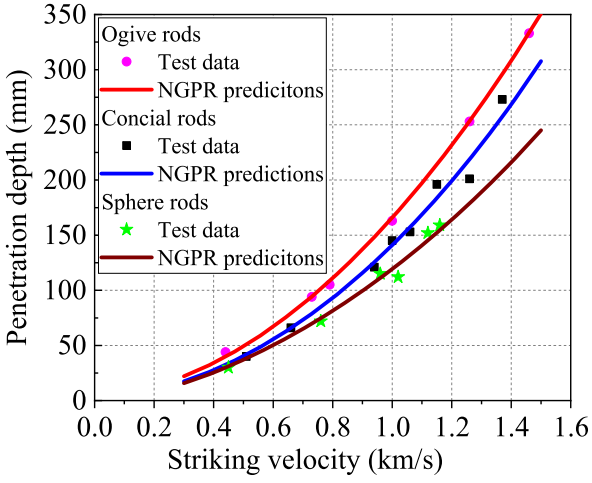

Fig. 7. The depth measurements of penetration Al6061 [12] and the predictions from the NGPR formula for different nose shapes.

Table 2
Optimized parameters of GPR and NGPR formulae for penetration concretes with different unconfined compressive strengths.

Target species	Formula	*A*	*B*	*C*	*D* ($\overline{D}$)
47.6 MPa [24]	NGPR	8.38	1.03	2.01	0.02
	GPR	10.27	1.00	0.00	11.09
23 MPa [17]	NGPR	5.43	1.30	1.79	0.00
	GPR	5.96	1.30	1.72	4.08
39 MPa [17]	NGPR	6.85	1.30	2.05	0.02
	GPR	6.36	1.25	2.74	0.00
51 MPa [19]	NGPR	9.47	1.28	2.39	0.02
	GPR	11.27	1.00	0.00	12.82

Fig. 8 compares the predictions of the NGPR and GPR formulae and the experimental penetration depths of 47.6 MPa concrete. The experimental penetration depths from projectiles with 4.70 kg masses are used to calibrate the parameters of the NGPR and GPR formulae, and those parameters are utilized to predict the penetration depths for projectiles with masses of 4.3 kg and 0.32 kg. It can be seen that the NGPR formula can better reflect the changing trend of the test data than the GPR formula, and the former can significantly improve the predictions of penetration depth at the high velocity. The good agreement between the predictions by the NGPR formula and test data also demonstrates that the parameters calibrated by one group of test data can properly predict the penetration depths in other penetration cases. In Fig. 9, the experimental time-deceleration history at the striking velocity of 841 m/s by Feng et al. [24] and the other six time-deceleration histories from their numerical simulation are utilized to compare with predictions from the NGPR and GPR formulae to further interpret the performance of the two formulae. It is obvious that both the NGPR and GPR formulae can properly reflect the deceleration histories data. On the whole, the NGPR formula can better predict the penetration depth of the projectile with different masses at different striking velocities than the GPR model, and the former is also able to reasonably reflect the deceleration histories of the projectile. This point can be further validated by the penetration events of 39 MPa concrete as shown in Figs. 10 and 11(a-f) which also provides the comparison of the experimental penetration depths and time-deceleration histories data with model predictions. From Fig. 11(a–f), predictions by NGPR and GPR formulae both exhibit closer agreement with the experimental deceleration histories than that by Forrestal's form in Ref. [17]. In addition, the NGPR and GPR formulae are further checked by using the experimental penetration depth and time-deceleration historical data for 23 MPa concrete penetration events, as shown in Figs. 12 and 13(a-f). In Fig. 12, the experimental penetration depths with projectile of 3.0 CRH are utilized to calibrate the parameters of the NGPR and GPR formulae, and those parameters are utilized to predict the penetration depths for projectiles of 6.0 CRH. Fig. 13 (a–f) only presents the predicted deceleration histories of the NGPR formula due to the coincidence of the predictions of the GPR formula with that of the NGPR formula. Obviously, in this penetration event, the predictions by the NGPR formula are more consistent with the test penetration depths than that by the GPR formula while both exhibit similar predicted performance in deceleration histories. Finally, the experimental penetration depth measurements of 51 MPa concrete are employed to check the performance of the NGPR and GPR formulae, as shown in Fig. 14. It is observed that the NGPR obviously improves the predicted accuracy on penetration depths at high velocities.

From the above penetration events including both aluminum alloy and concrete targets, it can be concluded that the NGPR formula is more flexible and possess a better performance in predicting the motion of the projectile than the GPR formula. Besides, it is

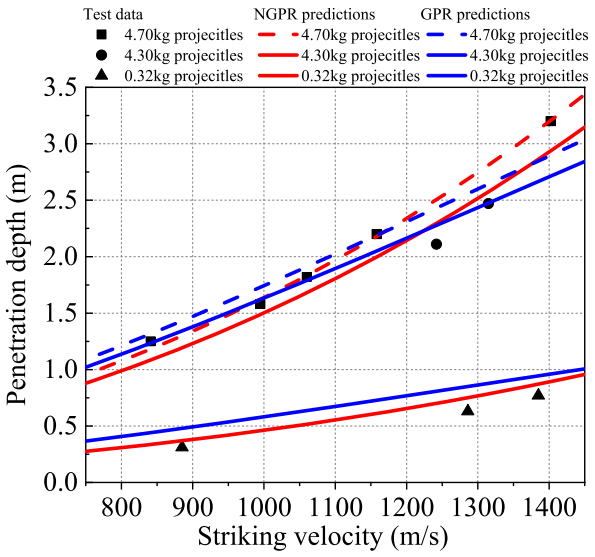

Fig. 8. The penetration depth data of 47.6 MPa concrete [27] and the predictions from the NGPR and GPR formulae.

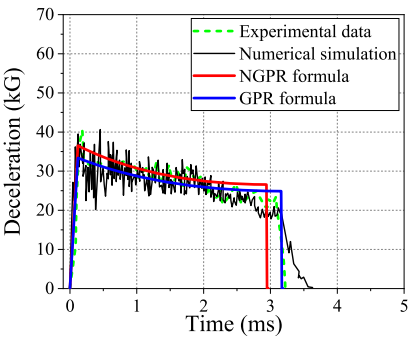

(a) v_s=841 m/s

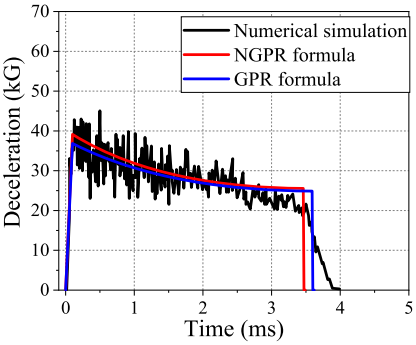

(b) v_s=995 m/s

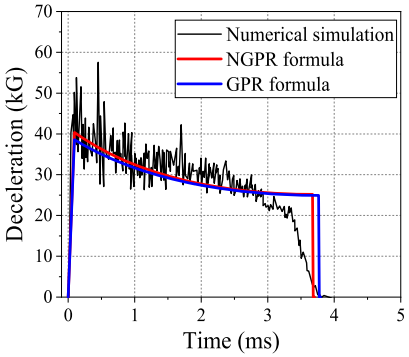

(c) v_s=1060 m/s

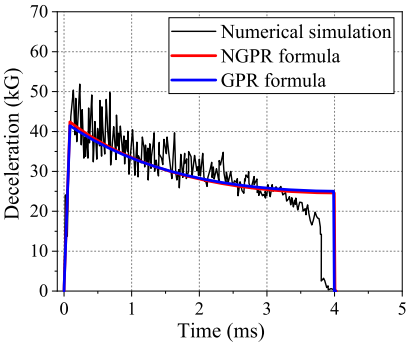

(d) v_s=1158 m/s

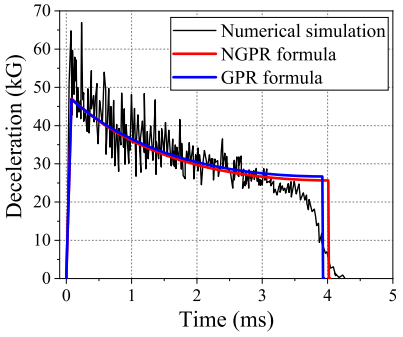

(e) v_s=1242 m/s

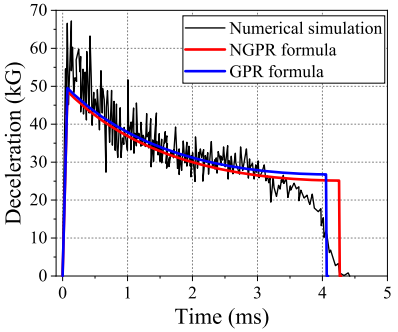

(f) v_s=1315 m/s

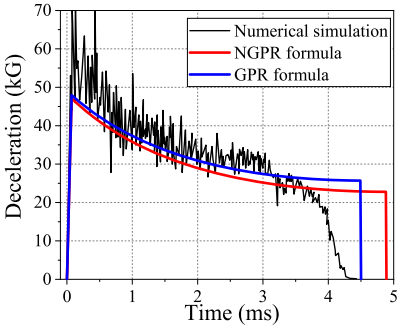

(h) v_s=1402 m/s

Fig. 9. The deceleration versus time data of 47.6 MPa concrete [24] and the predictions from the NGPR and GPR formulae.

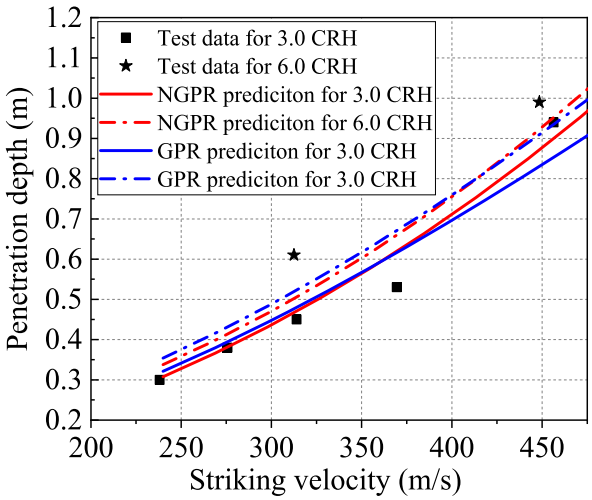

Fig. 10. The penetration depth data of 39 MPa concrete [17] and the predictions from the NGPR and GPR formulae.

indicated that this modified general penetration resistance and setting the parameter n equal to 1.0 are reasonable for all the penetration events investigated here.

5. Discussion

One should be noted that our study falls in the category of rigid penetration. Based on this premise, all the kinetic energy of the projectile is used to expand the hole and promote the flow of the target. Following the viewpoint by Chen et al. [16], the increase in the striking velocity of the projectile will induce a stronger flow of the target, and thus lead to a larger additional mass and a deeper penetration depth. The above trend between the penetration depth and striking velocity is also clearly evident in the experimental data of Figs. 5, 6, 8 and 14, all those figures embody a faster increase in penetration depth with the striking velocity. There exists an upper limit of the striking velocity under the assumption of the rigid projectile. Beyond this transition point, the projectile body begins to have obvious deformation, part of the kinetic energy of the projectile body is consumed for its own deformation. In this case, the penetration depth increases slowly with the striking velocity, and sometimes no increase in penetration depth occurs, a real example of this can be reflected in Fig. 6 of [23], this penetration process pertains to the semi-hydrodynamic penetration field. Thus, if the projectile can not be regarded as a rigid body, the assumption that the additional mass monotonically increases with the striking velocity will be not suitable, this is because this assumption can result in an overestimation of the penetration depth. In other words, the rigid penetration is the premise for the assumption that the additional mass monotonically increases with the striking velocity to be valid.

Besides, it is necessary to mention the phenomena of cavitation. As reported by Hill [31], the cavitation expansion of the target can absorb an appreciable amount of kinetic energy of the projectile, thus diminishing the penetration performance of the kinetic projectile. Generally, the published penetration experiments that the common kinetic projectile penetrated the concrete and metals hardly induce the cavitation of the target. This is because the critical cavitation velocity is relatively high, and the corresponding high stress in the projectile body exceeds the elastic stress level, which causes severe deformation and even failure, thus influencing the occurrence of the cavitation. However, with the development of high-strength projectiles, the cavitation of the metal and concrete target may be realized in the coming years. Here, we assume that the projectile remains rigid at any velocities, it can be inferred that as the striking velocity of the projectile increases, the penetration depth firstly exhibits a rapid growth trend, as shown in the experimental data in Figs. 5, 6, 8 and 14, but when the penetrating velocity approaches the cavitation velocity, this rapid growth trend of penetration depth will change due to a large amount of energy absorption by the cavitation of the target. Thus, the assumption that the additional mass monotonically increases with the striking velocity will be not proper around the cavitation velocity, although the projectile remains rigid, due to an overestimation of the penetration depth with this assumption. On the whole, it concludes that the assumption that the additional mass monotonically increases with the striking velocity is only valid in the condition of rigid penetration and below cavitation velocity.

By considering the effect of striking velocity and the projectile mass on the additional mass based on the general penetration resistance, a modified general penetration resistance of Eq. (23) is proposed. Then, this expression is used to formulate a semi-empirical formula denoted as the NGPR formula. To simplify the unknown parameters, the new parameter n is set to 1.0, which means that the additional mass is linearly related to the projectile kinetic energy. The good agreement of the predictions from the NGPR formula with all the experimental penetration data investigated here demonstrates that this modified general penetration resistance of Eq. (23) and the value of n equals 1.0 are reasonable. We should also emphasize the significance of deriving a physically-based relationship for the additional mass term through rigorous analytical modeling.

To explain the difference between the predictions of the NGPR formula, GPR formula and the cavity expansion model, the relation

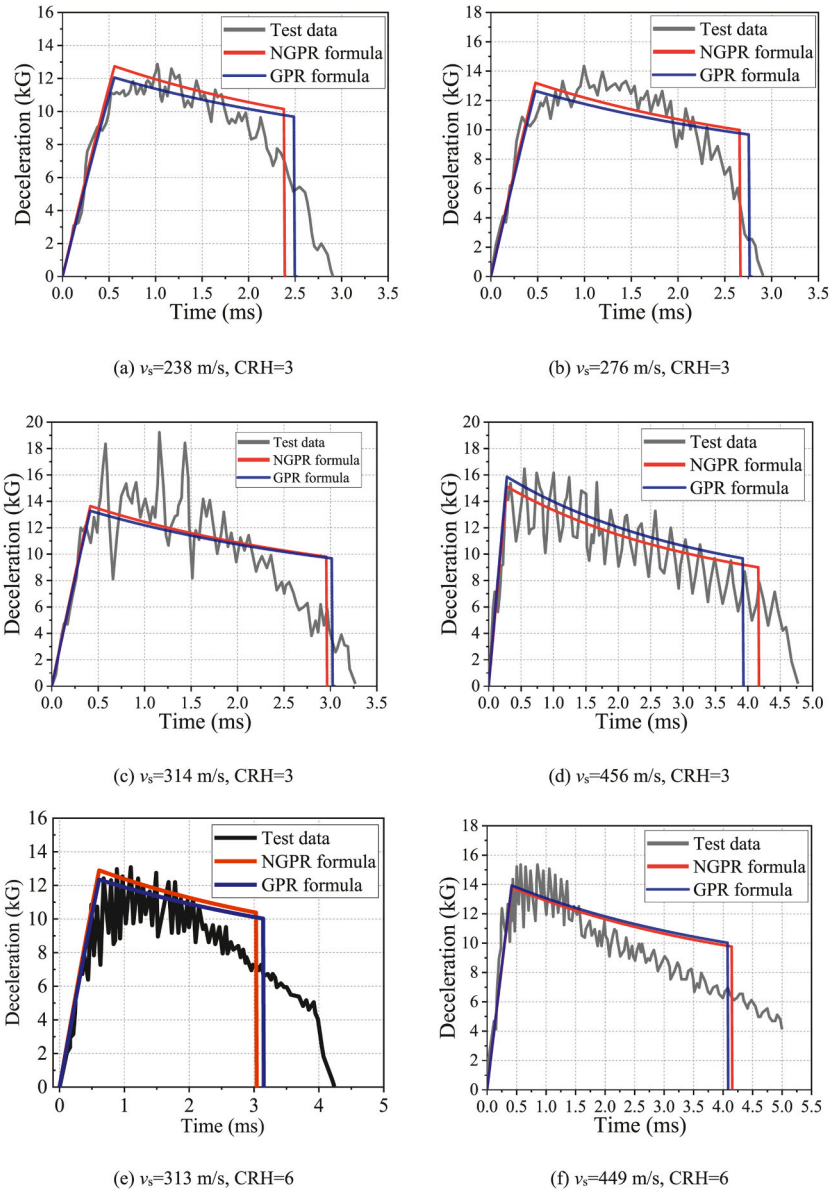

(a) v_s=238 m/s, CRH=3 (b) v_s=276 m/s, CRH=3

(c) v_s=314 m/s, CRH=3 (d) v_s=456 m/s, CRH=3

(e) v_s=313 m/s, CRH=6 (f) v_s=449 m/s, CRH=6

Fig. 11. The deceleration versus time data of 39 MPa concrete [17] and the predictions from the NGPR and GPR formulae.

of dimensionless stress with the dimensionless velocity gained by the NGPR formula, GPR formula and the cavity expansion model are compared. To this end, the total force acting on the projectile as expressed by Eq. (8) is rewritten. Eq. (8) is expressed as:

$$F_x = -M\frac{dv}{dt} = \frac{M}{M_m}\frac{\pi d^2}{4}\left(AYN_1 + B\rho v^2 N_2 + C\sqrt{\rho Y}\, vN_3\right)$$

Eq. (8) is rewritten as:

$$-M\frac{dv}{dt}\Big/\left(\frac{\pi d^2}{4}Y\right) = F_x\Big/\left(\frac{\pi d^2}{4}Y\right) = \sigma\Big/Y = \frac{M}{M_m}\left(AN_1 + B\frac{\rho v^2}{Y}N_2 + C\sqrt{\frac{\rho v^2}{Y}}N_3\right) \tag{25}$$

In Eq. (25) defining $\sigma = F_x/(\pi d^2/4)$ as the stress acting on the projectile, and σ/Y becomes the dimensionless stress. The $\sqrt{\rho v^2/Y}$ is the dimensionless penetrating velocity. As seen, Eq. (25) expresses the relation between the dimensionless stress and the dimensionless penetrating velocity. For the referenced cavity expansion models, the additional mass is not considered, thus M_m is equal to M. For the NGPR formula and GPR formula, the M_m is expressed as Eq. (24e) and Eq. (17e), respectively.

Fig. 15 provides the curves of dimensionless stress with the dimensionless penetrating velocity for two selected penetration events.

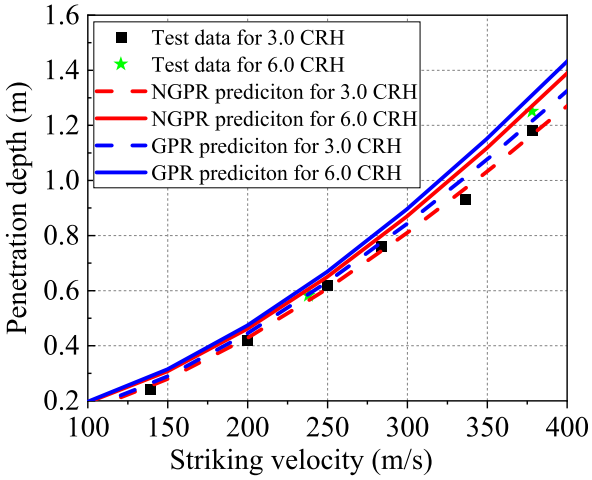

Fig. 12. The penetration depth data of 23 MPa concrete [17] and the predictions from the NGPR and GPR formulae.

Fig. 15(a) corresponds to the penetration event of Al6061 from Piekutowski et al. [26], who also provides values of A, B, and C from the cavity expansion model, ie., $A = 5.04$, $B = 0.983$, and $C = 0.94$. Fig. 15(b) corresponds to the penetration event of 51 MPa concrete [19]. In Ref. [19], values of A, B, and C from the cavity expansion model are 8.79, 1.12, and 1.60, respectively. Values of A, B, and C in the NGPR and GPR formulae are shown in Tables 1 and 2. Due to the assumption that the additional mass term M_m varies with the initial striking velocity, curves of dimensionless stress with the dimensionless penetrating velocity by the NGPR formula are different and separately depicted in Fig. 15. As seen from Fig. 15(a), curves of dimensionless stress with the dimensionless penetrating velocity by the NGPR formula under the striking velocity of 679 m/s and 966 m/s are close to that by the cavity expansion models, while the curve by the NGPR formula under the striking velocity of 1817 m/s is wholly lower than that by the cavity expansion model, thus the predicted depth by the NGPR formula is almost same as that by the cavity expansion model under the striking velocity of 679 m/s and 966 m/s but is larger under the striking velocity of 1817 m/s (Fig. 16(a)). Besides, curves by the NGPR formula under the striking velocity of 679 m/s and 966 m/s are first lower and then higher than that by the GPR formula with a resistance balance with each other, while the curve by the NGPR formula under the striking velocity of 1817 m/s is almost wholly lower than that by the GPR formula, thus the predicted depth by the NGPR formula is almost same as that by the GPR formula under the striking velocity of 679 m/s and 966 m/s but is larger under the striking velocity of 1817 m/s (Fig. 16(a)). The above regular is also reflected in Figs. 15(b) and Fig. 16(b) corresponding to the penetration event of 51Mpa concrete, it will not be discussed again. In short, different combinations of parameters corresponding to different models produce different resistance curves. The resistance curves of different models differ little at low strike velocity, but significantly at high strike velocity. As a result, the predicted penetration depths for different models are nearly coincident in low striking velocities but gradually diverge with the increase of the striking velocity, as shown in Fig. 16.

The main difference between the proposed NGPR formula, the GPR formula and Forrestal's form is the former can improve the predicted ability on penetration depths at high velocities. With the development of extremely high-strength projectiles, the upper-velocity limit of rigid penetration can be largely enhanced, in this case, the superiority of the proposed NGPR formula will be more evident. Besides, for the penetration case where the mechanical constitutive behavior of the target is complex and difficult to characterize by mathematical equations, the analytical method and numerical simulation may encounter obstacles. The semi-empirical formula becomes useful. With one group of penetration data points, the present NGPR formula can be used to obtain the total resistance and to predict the penetration data for other penetration cases, such as the projectiles with different nose shapes, the projectile with different masses or diameters as well as the projectiles with different striking velocities. This advantage is also helpful to reduce the number of experiments. It should be noted that, with more test data points, the calibrated parameters in the NGPR formula can more accurately reflect the target resistance.

6. Conclusion

The present paper is devoted to seeking a proper semi-empirical formula for predicting the motion of the rigid projectile during the deep penetration, due to the insufficient prediction of penetration depth and deceleration history of the commonly used Forrestal's form. To this end, firstly, the general penetration resistance is employed to formulate the semi-empirical formula (denoted as the GPR formula), due to the 'general' characteristic of the general penetration resistance. The performance of the GPR formula is checked by comparing with the individual test data, the results show that the GPR has the same predicted problem as Forrestal's form, they both can not predict well the experimental penetration depths in the high velocities of the rigid projectile. To solve this problem, the general penetration resistance is modified by the assumption that the additional mass of the rigid projectile should be increased with the striking velocity and the projectile mass. Then, the new semi-empirical formula based on this modified general penetration resistance (denoted as the NGPR formula) is established. The predictions of the NGPR formula exhibit good agreement with individual published experimental data of different projectiles and striking velocities as well as different targets, which also demonstrates the

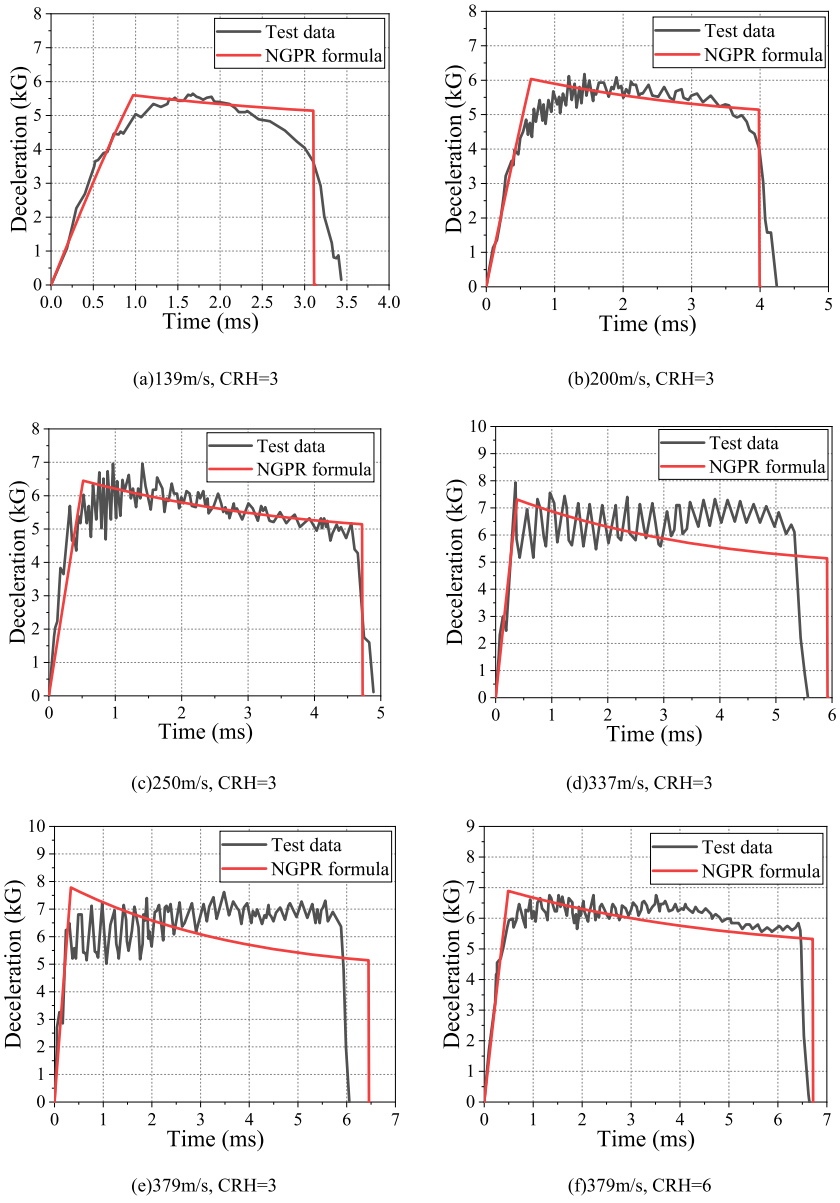

Fig. 13. The deceleration versus time data of 23 MPa concrete [17] and the predictions from the NGPR formula.

reasonableness of the assumption that the additional mass of the projectile increases with the striking velocity and the projectile mass. The superiority of the NGPR formula is the improvement of the prediction accuracy on penetration depths at high velocities of the rigid projectile compared to the GPR formula and the commonly used Forrestal's form, this may become more important with the development of the extremely high-strength projectiles and the elevation of the striking velocity. Besides, for the penetration case where the mechanical constitutive behavior of the target is complex and difficult to characterize by mathematical equations, the analytical method and numerical simulation may encounter obstacles. The semi-empirical formula becomes useful. With one group of penetration data points, the present formula can be used to obtain the total resistance and to predict the penetration data for other penetration cases with the merit of reducing the number of experiments.

Author contribution statement

Zhao Zhang: Conceived and designed the experiments; Performed the experiments; Analyzed and interpreted the data; Wrote the paper.

Yanqing Wu: Analyzed and interpreted the data; Contributed reagents, materials, analysis tools or data; Wrote the paper.

Fenglei Huang: Analyzed and interpreted the data; Contributed reagents, materials, analysis tools or data; Wrote the paper.

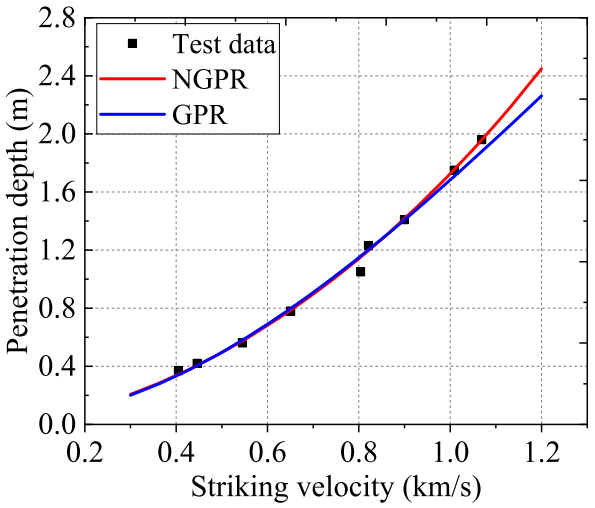

Fig. 14. The penetration depth data of 51 MPa concrete [19] and the predictions from the NGPR and GPR formulae.

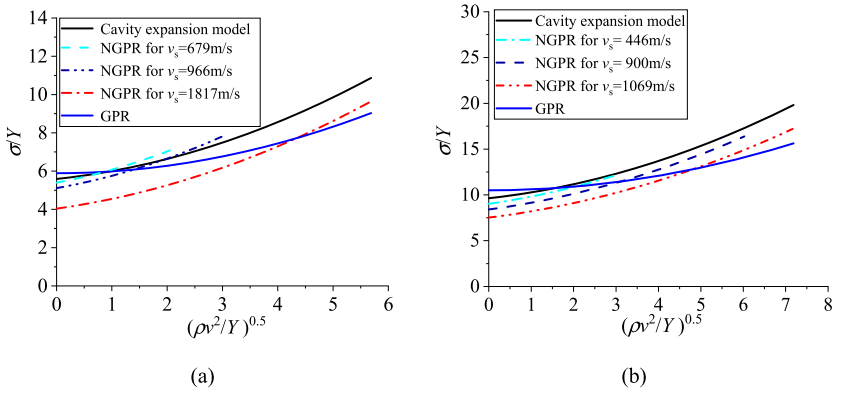

Fig. 15. The relations of dimensionless stress with the dimensionless penetrating velocity for the NGPR formula, GPR formula and the cavity expansion model in two penetration events, (a) the penetration of Al6061 [23], (b) the penetration of 51 MPa concrete [19].

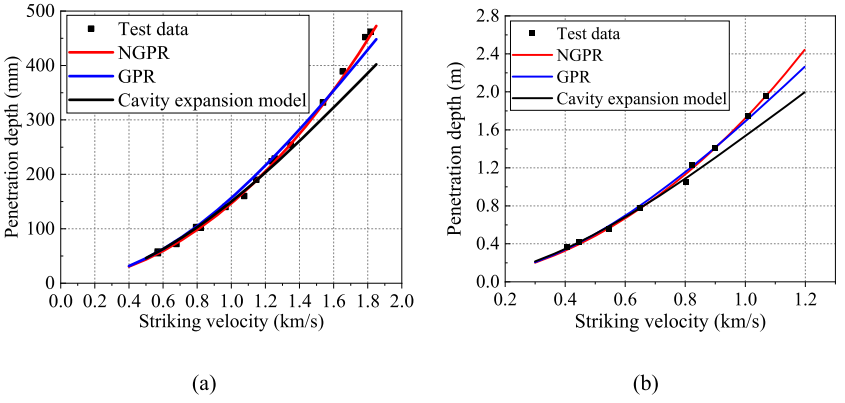

Fig. 16. Penetration depths predicted NGPR formula, GPR formula and the cavity expansion model in two penetration events: (a) the penetration of Al6061 [23], (b) the penetration of 51 MPa concrete [19].

Funding statement

Professor Yanqing Wu was supported by Innovative Research Group Project of the National Natural Science Foundation of China [11872119].

Data availability statement

Data will be made available on request.

Declaration of interest's statement

The authors declare no competing interests.

Appendix A

For the nose profile that can be expressed by the general convex function $y = y(x)$ as shown in Fig. 1, N_1, N_2, and N_3 are expressed as:

$$N_1 = 1 + \frac{8\mu_m}{d^2}\int_0^L y\mathrm{d}x \tag{A.1}$$

$$N_2 = N^* + \frac{8\mu_m}{d^2}\int_0^L \frac{yy'^2}{1+y'^2}\mathrm{d}x \tag{A.2}$$

$$N_3 = N^{**} - \frac{8\mu_m}{d^2}\int_0^L \frac{yy'^2}{\sqrt{1+y'^2}}\mathrm{d}x \tag{A.3}$$

where

$$N^* = \frac{4\iint_{A_n}\cos^3\theta\mathrm{d}A_s}{\pi d^2} = -\frac{8}{d^2}\int_0^L \frac{yy'^3}{1+y'^2}\mathrm{d}x \tag{A.4}$$

$$N^{**} = \frac{4\iint\cos^2\theta\mathrm{d}A_s}{\pi d^2} = \frac{8}{d^2}\int_0^L \frac{yy'^2}{\sqrt{1+y'^2}}\mathrm{d}x \tag{A.5}$$

Generally, the values of dimensionless parameters N_1, N_2, N_3 should be numerically integrated for a given nose profile function $y = y(x)$. For the commonly used ogival nose, conical nose and spherical nose in weapon engineering, N_1, N_2, and N_3 have explicit expression. For the ogival nose in Fig. A1(a):

$$N_1 = 1 + 4\mu_m\varphi^2\left[\left(\frac{\pi}{2}-\varphi_0\right) - \frac{\sin 2\varphi_0}{2}\right] \tag{A.6}$$

$$N_2 = N^* + \mu_m\varphi^2\left[\left(\frac{\pi}{2}-\varphi_0\right) - \frac{1}{3}\left(2\sin 2\varphi_0 + \frac{\sin 4\varphi_0}{4}\right)\right] \tag{A.7}$$

$$N^* = \frac{1}{3\varphi} - \frac{1}{24\varphi^2}, 0 < N^* \le \frac{1}{2} \tag{A.8}$$

$$\varphi_0 = \arcsin\left(1 - \frac{1}{2\varphi}\right), \quad \varphi \ge \frac{1}{2} \tag{A.9}$$

$$N_3 = N^{**} + 4\mu_m\varphi^2\left\{\frac{1}{2\varphi} - \frac{1}{3}\left[1 - \left(1 - \frac{1}{2\varphi}\right)^3\right]\right\} \tag{A.10}$$

$$N^{**} = 4\sqrt{\left(\frac{1}{\varphi} - \frac{1}{4\varphi^2}\right)}\left[\varphi^2 - \frac{1}{3}\varphi + \frac{1}{12}\right] - 4\left(\varphi^2 - \frac{\varphi}{2}\right)\sin^{-1}\sqrt{\left(\frac{1}{\varphi} - \frac{1}{4\varphi^2}\right)} \tag{A.11}$$

where $\varphi = s/d$ is the caliber-radius-heads of the ogival nose, s is the radius of the ogives nose and d is the shank diameters; μ_m is the sliding friction coefficient in impact.

For the conical nose in Fig. A1(b):

$$N_1 = 1 + 2\mu_m\varphi \tag{A.12}$$

$$N_2 = N^* + \frac{2\mu_m\varphi}{1+4\varphi^2} \tag{A.13}$$

$$N^* = \frac{1}{1+4\varphi^2}, \quad 0 < N^* \le 1 \tag{A.14}$$

$$N_3 = N^{**} + \frac{2\mu_m\varphi}{\sqrt{1+4\varphi^2}} \tag{A.15}$$

$$N^{**} = \frac{1}{\sqrt{1+4\varphi^2}} \tag{A.16}$$

where $\varphi = s/d$, s is the length of the conical nose and d is the shank diameters; μ_m is the sliding friction coefficient in impact.

For the spherical nose in Fig. A1(c):

$$N_1 = 1 + 2\mu_m\varphi^2(2\varphi_0 - \sin 2\varphi_0) \tag{A.17}$$

$$N_2 = N^* + \mu_m\varphi^2\left(\varphi_0 - \frac{\sin 4\varphi_0}{4}\right) \tag{A.18}$$

$$N^* = 1 - \frac{1}{8\varphi^2}, \quad \frac{1}{2} \le N^* \le 1 \tag{A.19}$$

$$\varphi_0 = \arcsin\left(\frac{1}{2\varphi}\right), \quad \varphi \ge \frac{1}{2} \tag{A.20}$$

$$N_3 = N^{**} + \frac{\mu_m}{3\varphi} \tag{A.21}$$

$$N^{**} = \frac{8\varphi^2}{3}\left[1 - \left(1 - \frac{1}{4\varphi^2}\right)^{\frac{3}{2}}\right] \tag{A.22}$$

where $\varphi = s/d$, s is the radius of the spherical nose and d is the shank diameters; μ_m is the sliding friction coefficient in impact.

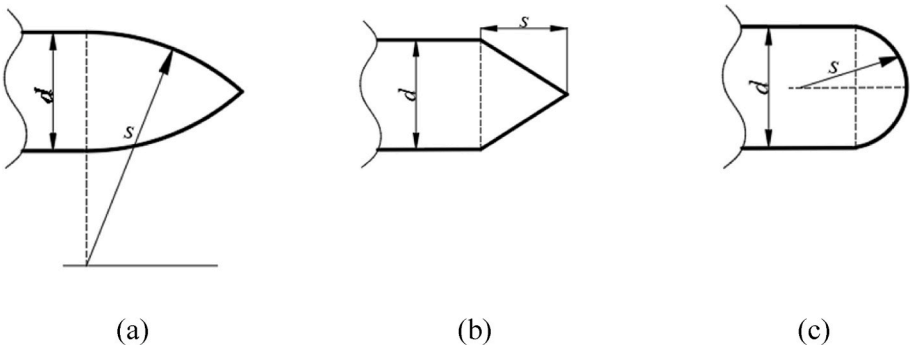

Fig. A1. Schematic of (a) ogive nose, (b) conical nose, (c) semi-sphere nose projectiles

References

[1] D.Z. Yankelevsky, Resistance of a concrete target to penetration of a rigid projectile - revisited, Int. J. Impact Eng. 106 (2017) 30–43, https://doi.org/10.1016/j.ijimpeng.2017.02.021.
[2] A. Murthy, G. Palani, N. Iyer, Impact analysis of concrete structural components (review paper), Defence Sci. J. 60 (2010) 307–319, https://doi.org/10.14429/dsj.60.358.
[3] D.Z. Yankelevsky, V.R. Feldgun, Y.S. Karinski, Concrete target quasi-static resistance to a penetrating projectile considering the material constitutive relationships, Int. J. Impact Eng. 156 (2021), 103959, https://doi.org/10.1016/j.ijimpeng.2021.103959.
[4] H. Wu, Y.C. Li, Q. Fang, Y. Peng, Scaling effect of rigid projectile penetration into concrete target: 3D mesoscopic analyses, Construct. Build. Mater. 208 (2019) 506–524, https://doi.org/10.1016/j.conbuildmat.2019.03.040.
[5] Z. Rosenberg, R. Kositski, Modeling the penetration and perforation of concrete targets by rigid projectiles, Int. J. Protective Struct 7 (2) (2016) 157–178.
[6] G. Ben-Dor, A. Dubinsky, T. Elperin, High-Speed Penetration Dynamics, World Scientific, 2012.

[7] Z. Rosenberg, E. Dekel, A comment on "The effect of target inertia on the penetration of aluminum targets by rigid ogive-nosed long rods" by T. L. Warren, Int. J. Impact Eng. 93 (2016), https://doi.org/10.1016/j.ijimpeng.2016.02.009.
[8] T. Warren, Response to: a comment on "The effect of target inertia on the penetration of auminum targets by rigid ogive-nosed long rods" by T.L. Warren, Int. J. Impact Eng. 93 (2016), https://doi.org/10.1016/j.ijimpeng.2016.03.002.
[9] Z. Rosenberg, R. Kositski, E. Dekel, Comment on: "Rigid and eroding projectile penetration into concrete targets based on an extended cavity expansion model" by Kong et al, Int. J. Impact Eng. 104 (2017), https://doi.org/10.1016/j.ijimpeng.2017.03.004.
[10] X. Kong, W. Hao, Q. Fang, Y. Peng, Response to: comment on "Rigid and eroding projectile penetration into concrete targets based on an extended cavity expansion model" by Kong et al, Int. J. Impact Eng. 104 (2017), https://doi.org/10.1016/j.ijimpeng.2017.03.003.
[11] D.Z. Yankelevsky, V.R. Feldgun, Issues in modelling the penetration of thick targets by rigid long rods, Int. J. Impact Eng. 137 (2020), 103474, https://doi.org/10.1016/j.ijimpeng.2019.103474.
[12] M.J. Forrestal, K. Okajima, V.K. Luk, Penetration of 6061-t651 aluminum targets with rigid long rods, J. Appl. Mech. 55 (4) (1988) 755–760, https://doi.org/10.1115/1.3173718.
[13] J.V. Poncelet, Cours De Mechanique Industrielle, first ed., 1829.
[14] L. Petry, Monographies de Systemes d'Artillerie, Brussels, 1910.
[15] T.L. Warren, M.J. Forrestal, Effects of strain hardening and strain-rate sensitivity on the penetration of aluminum targets with spherical-nosed rods, Int. J. Solid Struct. 35 (28) (1998) 3737–3753, https://doi.org/10.1016/S0020-7683(97)00211-4.
[16] X.W. Chen, X.L. Li, F.L. Huang, H.J. Wu, Y.Z. Chen, Damping function in the penetration/perforation struck by rigid projectiles, Int. J. Impact Eng. 35 (11) (2008) 1314–1325, https://doi.org/10.1016/j.ijimpeng.2007.07.011.
[17] M.J. Forrestal, D.J. Frew, J.P. Hickerson, T.A. Rohwer, Penetration of concrete targets with deceleration-time measurements, Int. J. Impact Eng. 28 (5) (2003) 479–497, https://doi.org/10.1016/S0734-743X(02)00108-2.
[18] D.J. Frew, S.J. Hanchak, M.L. Green, M.J. Forrestal, Penetration of concrete targets with ogive-nose steel rods, Int. J. Impact Eng. 21 (6) (1998) 489–497, https://doi.org/10.1016/S0734-743X(98)00008-6.
[19] M.J. Forrestal, D.J. Frew, S.J. Hanchak, N.S. Brar, Penetration of grout and concrete targets with ogive-nose steel projectiles, Int. J. Impact Eng. 18 (5) (1996) 465–476, https://doi.org/10.1016/0734-743X(95)00048-F.
[20] D.J. Frew, M.J. Forrestal, J.D. Cargile, The effect of concrete target diameter on projectile deceleration and penetration depth, Int. J. Impact Eng. 32 (10) (2006) 1584–1594, https://doi.org/10.1016/j.ijimpeng.2005.01.012.
[21] D.J. Frew, M.J. Forrestal, S.J. Hanchak, Penetration experiments with limestone targets and ogive-nose steel projectiles, J. Appl. Mech. 67 (4) (2000) 841–845, https://doi.org/10.1115/1.1331283.
[22] M.J. Forrestal, S.J. Hanchak, Penetration limit velocity for ogive-nose projectiles and limestone targets, J. Appl. Mech. 69 (6) (2002) 853–854, https://doi.org/10.1115/1.1480820.
[23] A.J. Piekutowski, M.J. Forrestal, K.L. Poormon, T.L. Warren, Penetration of 6061-T6511 aluminum targets by ogive-nose steel projectiles with striking velocities between 0.5 and 3.0 km/s, Int. J. Impact Eng. 23 (1, Part 2) (1999) 723–734, https://doi.org/10.1016/S0734-743X(99)00117-7.
[24] J. Feng, M. Song, W. Sun, L. Wang, W. Li, W. Li, Thick plain concrete targets subjected to high speed penetration of 30CrMnSiNi2A steel projectiles: tests and analyses, Int. J. Impact Eng. 122 (2018) 305–317, https://doi.org/10.1016/j.ijimpeng.2018.09.005.
[25] D. Yankelevsky, V. Feldgun, The embedment of a high velocity rigid ogive nose projectile into a concrete target, Int. J. Impact Eng. 144 (2020), 103631, https://doi.org/10.1016/j.ijimpeng.2020.103631.
[26] M. Forrestal, N. Brar, V. Luk, Penetration of strain hardening targets with rigid spherical-nose rods, J. Appl. Mech. 58 (1991), https://doi.org/10.1115/1.2897183.
[27] M.J. Forrestal, V.K. Luk, Z. Rosenberg, N. Brar, Penetration of 7075-T651 aluminum targets with ogival-nose rods, Int. J. Solid Struct. 29 (1992) 1729–1736, https://doi.org/10.1016/0020-7683(92)90166-Q.
[28] M.J. Forrestal, D.Y. Tzou, A spherical cavity expansion penetration model for concrete targets, Int. J. Solid Struct. 34 (1997) 4127–4146, https://doi.org/10.1016/S0020-7683(97)00017-6.
[29] Z. Rosenberg, Y. Vayig, On the friction effect in the perforation of metallic plates by rigid projectiles, Int. J. Impact Eng. 149 (2021), 103794. https//doi.org/10.1016/j.ijimpeng.2020.103794.
[30] Z. Rosenberg, Y. Vayig, The effect of friction on the shanks of rigid projectiles penetrating concrete targets, Int. J. Impact Eng. 156 (2021), 103926, https://doi.org/10.1016/j.ijimpeng.2021.103926.
[31] R. Hill, Cavitation and the influence of headshape in attack of thick targets by non-deforming projectiles, J. Mech. Phys. Solids 28 (1980) 249–263, https://doi.org/10.1016/0022-5096(80)90019-8.